Lattice vibrations in δ-plutonium: Molecular dynamics calculation

M. I. Baskes, A. C. Lawson, and S. M. Valone
Los Alamos National Laboratory, Los Alamos, New Mexico 87545, USA
(Received 10 January 2005; revised manuscript received 11 April 2005; published 28 July 2005)

Analysis of previous experimental neutron diffraction measurements has shown that the amplitude of lattice vibrations in δ-Pu alloys increases more rapidly than linearly with temperature. Using a recently developed Modified Embedded Atom Method (MEAM) potential for the Pu-Ga system, molecular dynamics (MD) calculations show an almost linear increase of the lattice vibrations with temperature. However, these same MD calculations show that the predicted neutron diffraction peak intensities vary with temperature in a nonlinear fashion similar to experiment. By using two MEAM models of Pu, the first including both itinerant and localized f-electron behavior and the second, identical to the first, but with the itinerant f-electron behavior suppressed, this non-Debye behavior is shown to arise directly from the Pu itinerant f-electrons in the model and the resultant metastability of δ-Pu.

DOI: 10.1103/PhysRevB.72.014129 PACS number(s): 61.12.−q, 63.70.+h, 63.10.+a

I. INTRODUCTION

From a structural point of view, Pu and Ga are two of the most interesting elements in the Periodic Table. Pure Pu contains six solid phases at ambient pressure, as well as the liquid phase at various temperatures. Complicating our understanding of Pu is the fact that the f-electrons seem to change their character between the different crystal structures from itinerant to localized behavior. These changes manifest themselves in the curious situation that the close packed fcc phase, δ-Pu, has the largest volume per atom of all of the phases. Similarly, Ga has five solid phases as a function of pressure and temperature. Alloying of Pu with Ga significantly increases the temperature range of stability of this phase, specifically with respect to the ground state α -Pu. However, the stabilization is of a metastable nature, relying on the slow kinetics at ambient temperature.[1] At ambient pressures, and below 400 K, Ga-stabilized δ-Pu at equilibrium would decompose into α-Pu and Pu_3Ga. We view the phase metastability as another manifestion of the changeable nature of the f-electrons in Pu. Background information for those not familiar with the Pu-Ga system may be obtained in Los Alamos Science.[2]

Not only are Pu and Ga scientifically challenging, they are of extreme importance to the nuclear weapons community, especially in the light of our recent commitment to being able to accurately predict stockpile aging. Aging is inherently a process that depends upon atomistic mechanisms; thus a reliable atomic level model of the Pu/Ga system is key to our success.

The vibrations of both Pu and Ga atoms are a very simple property that appears to be quite different than in non-f-electron metals.[3–5] Lawson *et al.*[6,7] have extracted the mean square displacement (MSD) of the atoms in Pu-Ga alloys as a function of temperature from neutron diffraction spectra. In most metals the MSD increases linearly with temperature above the characteristic Debye temperature, implying that this Debye temperature is independent of temperature. However, for these alloys, the inferred MSD increases in a nonlinear fashion, implying that the effective Debye temperature decreases with increasing temperature. Such behavior indicates a weaking of bonds at higher temperature. The underlying cause of this behavior is not known with certainty. The elastic softening of δ-Pu found by Debye-Waller factor measurements is quantitatively supported by ultrasonic measurements.[8–10]

Theoreticians have been frustrated for the past few years in their inability to capture the physics of δ-Pu using density functional methods that work well for essentially all of the other elements.[11] For over the last decade it has been shown that many-body semiempirical potentials typified by the Embedded Atom Method (EAM) have been able to represent the physical properties of a significant number of metals and alloys in excellent agreement with experiment.[12,13] More recently the EAM has been supplemented with angular forces leading to potentials that cover most of the Periodic Table, including elements such as silicon[14,15] and tin[16] where angular forces are extremely important. Our model of tin[16] has been a splendid success in its ability to predict the phase stability and thermodynamics in quantitative agreement with experiment.

The modified EAM (MEAM) formalism has been applied to Pu,[17] Ga,[18] and the Pu-Ga system.[19] In the present work we will use slightly altered MEAM parameters from our previous work to calculate the vibrational properties of Pu-Ga alloys and compare the results to the previously published experiments discussed above. In particular, the metastability of Ga-stabilized δ-Pu is preserved in the present parameter set. From these calculations, we hope to gain understanding of the unusual behavior of these Pu-Ga alloys. In the next section, we will discuss the specific MEAM potentials we use, the simulation details, and basic diffraction theory. The following section will briefly present the previous experimental results. The bulk of the paper is a discussion of the simulation results and the comparison to experiment. Our major result is that the predicted MSD is linear in temperature, in apparent conflict with experiment. On the contrary, our predicted diffraction intensities vary nonlinearly with temperature, similarly to experiment. We attribute this apparent conflict to inherent assumptions in the experimental analysis technique.

TABLE I. Parameters for the MEAM potentials. Values listed are the cohesive energy E^0 (eV), the equilibrium nearest neighbor distance r^0 (Å), the exponential decay factor for the universal energy function α, the short range correction factor δ, the scaling factor for the embedding energy A, the exponential decay factors for the atomic densities $\beta^{(l)}$, the weighting factors for the atomic densities $t^{(l)}$, and the density scaling factor ρ^0.

	E^0	r^0	α	δ	A	$\beta^{(0)}$	$\beta^{(1)}$	$\beta^{(2)}$	$\beta^{(3)}$	$t^{(1)}$	$t^{(2)}$	$t^{(3)}$	ρ^0
Pu	3.800	3.280	3.31	0.460	1.10	2.35	1.0	6.0	9.0	2.00	4.07	−0.61	1.0
Ga	2.897	3.004	4.42	0.097	0.97	4.80	3.1	6.0	0.5	2.70	2.06	−4.00	0.7
PuGa	4.104	3.190	4.60	0.300	⋯	⋯	⋯	⋯	⋯	⋯	⋯	⋯	⋯

To develop an understanding of the source of the nonlinear behavior of the diffraction intensities, we create a second MEAM model of Pu with the itinerant f-electrons suppressed. Using this model, the nonlinear behavior in the diffraction intensities disappears. Thus the nonlinearities are shown to arise from the presence of the itinerant f-electrons in Pu. We conclude with a short summary.

II. THEORY

A. Potentials

The EAM formulation is well known[12,13] and will not be repeated here. Similarly the MEAM has also been fully documented in the literature.[20,21] The parameters used are given in Table I. The potential development follows closely that used in Baskes.[22] Angular screening as implemented in Baskes *et al.*[21] was used to limit the range of the pair and density functions. The parameters used are given in Table II. In addition, a radial cutoff of 4.1 Å was used to facilitate computation. The use of larger cutoff values does not change the results presented here.

A more physically based calculation of the partial electron density has been implemented,

$$\rho_i^{(h)^2} = \frac{\sum_j \rho_j^{(0)}(R_{ij})}{\sum_j t_j^{(h)^2}\rho_j^{(0)}(R_{ij})} \sum_j t_j^{(h)}\rho_j^{a(h)}(R_{ij}) \sum_k t_k^{(h)}\rho_k^{a(h)}(R_{ik}) \times P_h^0(\cos(\theta_{jik})), \quad (1)$$

where $\rho_j^{a(h)}$ are the atomic electron densities for angular momentum state h, P_h^0 is the 0th order Legendre polynomial, R_{ij} is the distance between atoms i and j, and θ_{jik} is the included angle between atoms j, i, and k. The previous formalism[20] included contributions to the partial electron density from an atom even when its weighting factor t was zero. This formalism leaves the model unchanged for a single component system.

We have previously discussed the importance of the f-electrons in the development of radiation damage in Pu (Ref. 23) and vacancy mobility.[24] In that work we examined two related models: model I, a model essentially as described above; and model II, model I with the Pu itinerant f-electron behavior suppressed by setting $t_{\mathrm{Pu}}^{(3)}=0$. In Model I $t_{\mathrm{Pu}}^{(3)}<0$ and $\beta_{\mathrm{Pu}}^{(3)}$ is very large, representing a reduced contribution of localized f-electrons relative to our reference state. By increasing $t_{\mathrm{Pu}}^{(3)}$ from its value of −0.61 in Model I to 0.0 in Model II, we are adding localized f-electrons and consequently removing itinerant f-electrons. Model I encompasses our best representation of the complex behavior of Pu, while model II is our approximation of how we feel Pu would act in the absence of itinerant f-electrons, a behavior much more similar to a fcc transition element. The model I parameters retain the metastability of the δ-phase relative to the α-phase. Setting $t_{\mathrm{Pu}}^{(3)}=0$ in model II removes any sensitivity to breaking inversion symmetry in the δ-crystal structure, the primary mechanism in the model by which the δ-phase metastability manifests itself. Simulations will be presented below using both of these models.

B. Simulation details

The simulations presented below used standard techniques. Essentially all calculations employed a 3D periodic, cubic cell of 256 atoms. An initial cell of Pu atoms arranged on fcc lattice sites with the equilibrium 0 K lattice constant of Pu was created. The desired concentration of Ga was obtained by randomly replacing the Pu atoms with Ga atoms. The cell was equilibrated using molecular dynamics for 10 ps using a time step of 1–2 fs under constant temperature and pressure (=0) using a Nosé-Hoover thermostat[25,26] with a time constant of 0.1 ps and Parrinello-Rahman[27] boundary conditions. Then using the equilibrated cell, a *NVT* (constant number, volume, and temperature) calculation was performed for 10 ps, saving configurations every 0.1 ps. The maximum average pressure of all of the *NVT* simulations performed was 0.2 GPa and typically the average pressure was an order of magnitude lower than this value. Temperature control was excellent with the average temperature being <0.1 K from the target and the root mean square (RMS)

TABLE II. Angular screening parameters for the MEAM potentials.

	Pu-Pu-Pu	Pu-Ga-Pu	Ga-Pu-Pu	Ga-Ga-Pu	Ga-Pu-Ga	Ga-Ga-Ga
$C_{\max}$	2.80	2.80	2.80	2.00	2.80	2.80
$C_{\min}$	1.75	2.00	2.00	1.40	2.00	1.40

deviation of temperature <1 K. Averages were performed using these 100 configurations for each Ga concentration. Tests were performed to show that the cell size and sampling procedure did not significantly affect the results presented below.

Two averages are presented below. The mean square displacement (MSD) of an atom from its average vector position $\bar{R}$ is given by

$$\langle u^2 \rangle = \frac{1}{NM} \sum_{i=1}^{M} \sum_{l=1}^{N} |R_l^i - \overline{R_l}|^2,$$

$$\overline{R_l} = \frac{1}{M} \sum_{i=1}^{M} R_l^i, \tag{2}$$

where the sums are performed over the vector position R_l^i of atom l in the ith configuration of the M configurations sampled. There are N scatterers.

The second average, the square of the structure factor at scattering vector K, is given by

$$\langle F^2 \rangle = \frac{1}{M} \sum_{i=1}^{M} \left| \frac{1}{N} \sum_{l=1}^{N} e^{-iK \cdot R_l^i} \right|^2. \tag{3}$$

Note that for multicomponent alloys, the above expression should have a different atomic scattering factor included for each type of atom. Conveniently, Pu and Ga have very similar scattering factors for the neutron diffraction experiments considered here. Thus, we are able to ignore the different scattering factors in this work. The simulations sampled K in ⟨100⟩, ⟨110⟩, and ⟨111⟩ directions in the range of 0–10 Å^{-1} using a step size of 0.1 Å^{-1}.

C. Diffraction intensity

Neutron diffraction is an effective tool that is commonly used to investigate vibrations in materials. The intensity of a diffracted neutron beam I at a scattering vector K and temperature T is given by[28]

$$I(K,T,N) = I_0(K,N) e^{-2W}. \tag{4}$$

The prefactor I_0 depends upon experimental conditions, the scattering vector, and the type and number N of scattering centers, but is temperature-independent. The temperature dependence of the diffracted intensity is captured by the Debye-Waller factor W given by

$$W = \frac{1}{2} \sum_q |K \cdot U_q|^2, \tag{5}$$

where U_q is the vector amplitude of the normal mode of wave vector q.

We can also calculate the scattered intensity directly from the structure factor[28]

$$I_{\text{calc}}(K,T,N) = I_1(K,N) \langle F^2 \rangle, \tag{6}$$

where the prefactor I_1 depends on the scattering vector and the number of scattering atoms for the simulation conditions. Hence the Debye-Waller factor is calculated from the simulations as

$$W = -\tfrac{1}{2} \ln \langle I_1 F^2 \rangle. \tag{7}$$

III. PREVIOUS EXPERIMENTAL RESULTS

Lawson *et al.*[6,7] have measured the neutron diffraction in two Pu-Ga alloys and used a Rietveld analysis with a single, average, isotropic Debye-Waller factor to extract the MSD. In the Debye model at temperatures above the Debye temperature, the Debye-Waller factor can be related to the MSD $\langle u^2 \rangle$ by

$$W = \frac{1}{2} \frac{\langle u_{\text{expt}}^2 \rangle}{3} K^2 \tag{8}$$

and the Debye temperature, in the limit of high temperature, is given by

$$\theta_D(T) = \sqrt{\frac{9\hbar^2}{mk} \frac{T}{\langle u_{\text{expt}}^2(T) \rangle}}, \tag{9}$$

where m is the atomic mass, $\hbar$ is Planck's constant over 2π, and k is the Boltzmann constant. Note that if $\langle u^2 \rangle$ is linear in temperature then the Debye temperature is indeed constant. For purposes of the discussion below, we will call alloys with such a linear Debye-Waller factor as Debye-type or Debye solids.

There are two important consequences of using Eq. (8) in the fitting of the diffraction data. First is the proportionality of W to K^2. This assumption is verified because the experimental data are fit well by the Rietveld analysis. The second assumption, that the coefficient of this proportionality is the MSD (within a constant factor) will be discussed in detail below.

Using this relationship, their results presented as $\langle u_x^2 \rangle = \langle u_y^2 \rangle = \langle u_z^2 \rangle = \langle u^2 \rangle / 3$ for the fcc δ-Pu alloys are reproduced in Fig. 1. We see here that the MSD is not linear as we would expect for a normal Debye solid, but includes a component that increases quadratically with increasing temperature. The lines through the experimental data are a quadratic fit in temperature and represent the data extremely well. The resultant R^2 for the quadratic fit was 0.9989 (0.9998) for the 2% (6%) data set. In contrast, a linear fit to the data is poor with R^2 values of 0.969 and 0.968 for the 2 data sets. Lawson *et al.*[6,7] modeled this behavior with a temperature-dependent Debye temperature.

IV. SIMULATION RESULTS AND DISCUSSION

A. Mean square displacement

The calculated MSD for both Pu and Ga atoms is shown in Fig. 1 for both models I and II. It is clear that for Ga atoms for both alloys, the MSD is essentially linear and independent of alloy composition. The resultant R^2 for the linear fit was 0.963 (0.986) for the 4.7% (9.8%) alloy. The data are noisier than the experimental data; hence the R^2 values are lower than the quadratic fits to the experimental data dis-

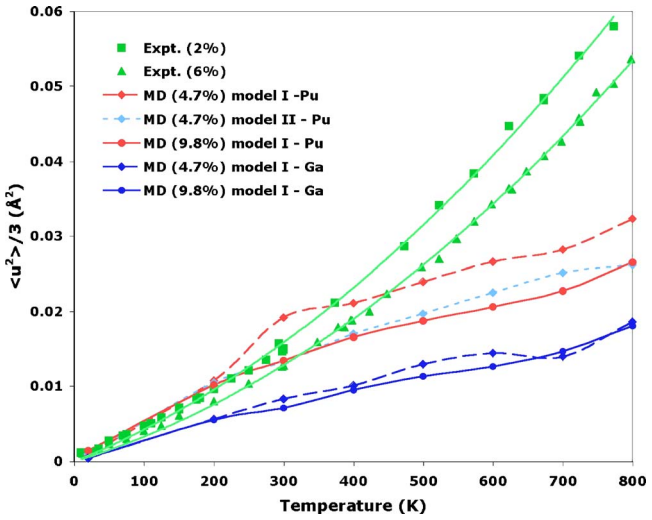

FIG. 1. (Color online) Average MSD in a cube axis direction vs temperature. Green symbols represent experimental values not differentiated by atom type. Red symbols (dark blue symbols) represent calculated values for Pu (Ga) in model I. Light blue symbols, dotted line represent calculated values for Pu using the MEAM model with itinerant *f*-electrons suppressed (model II).

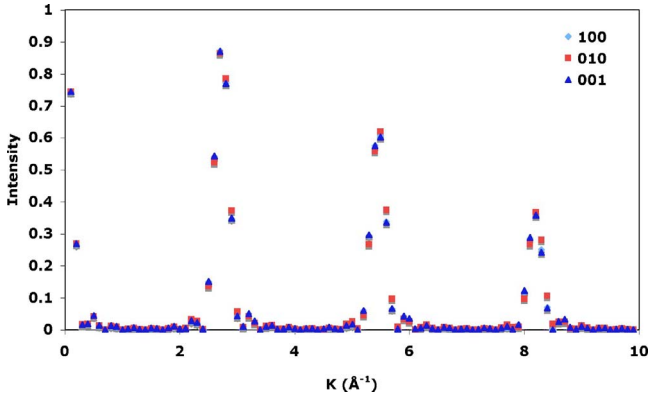

FIG. 2. (Color online) Calculated diffracted intensity (arbitrary units) as a function of the magnitude of the scattering vector *K*. Spectra were obtained from a simulation of a 9.8% alloy at 300 K and includes scattering vectors in three ⟨100⟩ directions.

cussed above. The standard deviation of the Pu MSD for the 4.7% alloy (model I) at 600 K (800 K) due to the statistics in the calculations was 0.0025 Å^2 (0.0011 Å^2). A quadratic fit to the Ga MSD yields slightly better R^2 values (0.973,0.990), but the resultant curvature for the 4.7% alloy is negative and that of the 9.8% alloy is very small. The MSD for Pu is a bit more complicated. The 9.8% alloy shows nearly linear behavior with a larger MSD than the Ga MSD. The resultant R^2 for a linear (quadratic) fit is 0.9899 (0.9905) using data for temperatures of 200 K and above. The resultant curvature for the quadratic fit is small and negative. The fact that the Pu MSD is larger than the Ga MSD is surprising since Pu has a much larger mass than Ga. A significantly smaller force constant between two Pu atoms than between a Pu and Ga atom can explain this result. Using neutron-resonance Doppler spectroscopy on a similar alloy, Lynn *et al.*[29] conclude that the Pu—Ga force constant is stiffer than the Pu-Pu force constant. Our result is consistent with the direction of forces they found, but requires a significantly higher force ratio. A direct calculation of the curvature of the potential well in the [100] direction for a Pu or Ga atom in a fully relaxed fcc Pu lattice at 0 K gives ~37% higher curvature for a Ga atom. Even this increase does not compensate for the 34 mass ratio of Pu:Ga. Perhaps our result is an anharmonic effect, as the MSD ratio appears to be smaller at lower temperatures.

More interesting behavior is found for the lower Ga concentration alloy. At the higher temperatures the MSD behavior is linear with a significant increase in MSD with decreasing Ga concentration. Using data at temperatures of 300 K and above, the R^2 for this alloy is 0.9880 (0.9917) for the linear (quadratic) fit. The resultant curvature for the quadratic fit is small and positive. The alloy effect is in the same direction as experiment and of the same approximate magnitude. As the temperature is lowered the 4.7% Ga alloy shows a sharp decrease in MSD below 300 K. We believe that this decrease is an indication of the instability of the δ-Pu phase. Decreasing amounts of Ga reduce the stability of δ-Pu relative to α-Pu. As further justification for this conjecture, we look at the results of the model II calculation. Here the MSD appears, as we would expect for a normal Debye solid. We fit our data to a linear function of temperature and use Eq. (8) to calculate the Debye temperature. We obtain values of 116 K (128 K) for the 4.7% (9.8%) Ga alloy using model I and 127 K for the 4.7% alloy using model II. These values are in reasonable agreement with those obtained experimentally for a 3.3% Ga alloy of 106 K using elastic constant data[30] and for a 5% Al alloy of 100 K using low temperature heat capacity data.[31]

Most critical for the purpose of this paper, none of the calculations exhibits the nonlinear increase of MSD with temperature observed by experiment. A quadratic fit to the calculated MSD data yields a curvature that is essentially zero. The remainder of this paper will attempt to explain the cause of this apparent disagreement.

B. Diffraction intensity

The analysis of the experimental neutron diffraction intensity employed Eq. (8), which is not necessarily valid. We now attempt to reanalyze the above experimental results by calculation of the diffracted neutron intensity directly from the MD simulations, obviating the use of Eq. (8). Typical calculated diffraction spectra are given in Fig. 2. Here we see the appearance of clear diffraction peaks at K values representative of the Bragg condition. The peaks for the three equivalent ⟨100⟩ directions show good agreement, implying that cubic symmetry exists for this sample. The existence of cubic symmetry was *not* found at all temperatures and alloy concentrations as expected from our previous investigation of pure Pu.[32] The peaks display a finite width due to the finite size of our sample.

We examined the size effect in two ways. First, we replicated our 256 atom cell in all three directions 2 and 4 times and recalculated the diffraction intensity for each new supercell. For each factor of 2 increase in cell dimension, the peak width was reduced by a factor of 2. The relative peak widths

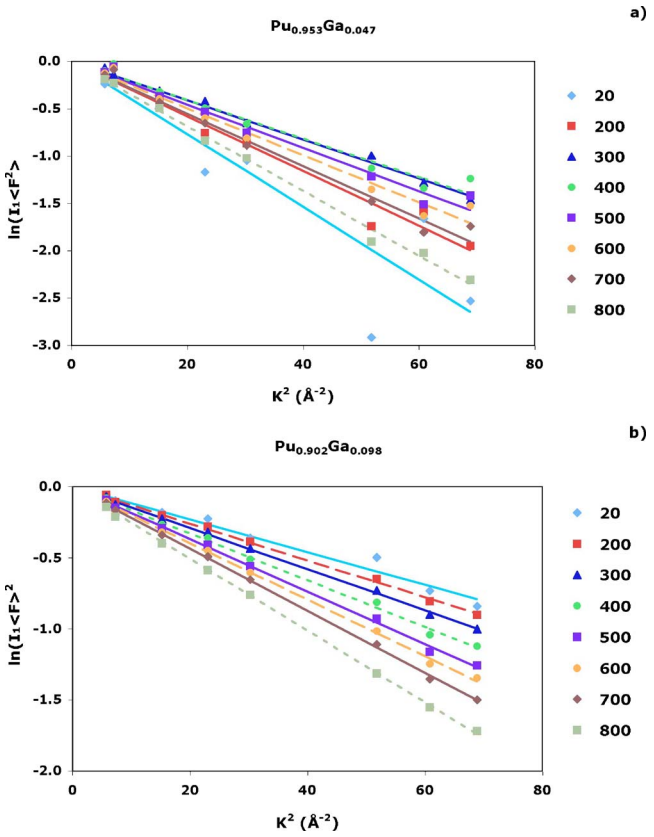

FIG. 3. (Color online) Calculated average diffracted intensity for the (a) 4.7% and (b) 9.8% alloy as a function of the square of the scattering vector, for various temperatures (K) indicated on the right of the figure. Points indicate the simulation values and lines indicate the linear fit.

(and heights) for different K directions did not change. Second, we sampled only atoms in a 7 Å sphere contained in our initial cubic cell. The relative peak widths (and heights) for different K vectors *did* change from our initial cubic cell. Thus, we conclude, as expected from diffraction theory, that our calculations contain the size and shape dependence contained in I_1 of Eq. (6).

We now examine the proportionality of the Debye-Waller factor to K^2 as predicted by Eq. (8). The calculated structure factors are scaled by a single intensity, I_1, for the complete data set, and fit to a linear function of K^2, forced to go through the origin. The results are presented in Fig. 3. At the higher Ga concentration [Fig. 3(b)] the fit is seen to be quite good. The data are linear in K^2 and extrapolates through the origin. At the lower Ga concentration [Fig. 3(a)] there appears to be much more scatter in the calculated intensities, but the K^2 dependence is clear. The intensity data for $T=20$ and 200 K have slopes more negative than that of the 300 K data, showing a reverse in the normal increase in intensity at lower temperatures. This behavior is caused by the phase transformation noted above. For this reason, we will not consider these two temperatures for the 4.7% alloy any further. The results shown in Fig. 3 clearly validate the K^2 dependence of Eq. (8).

The average intensity shown in this figure is an average of the integrated peak intensity over the peaks with the same

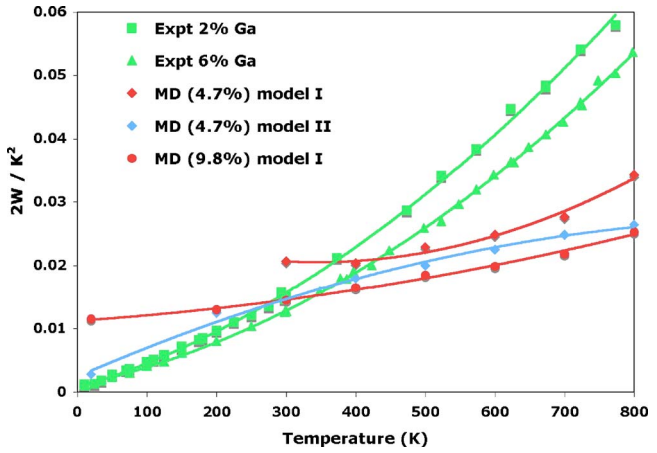

FIG. 4. (Color online) Calculated and experimental Debye-Waller factors scaled by the square of the scattering vector as a function of temperature. The lines are a quadratic fit for each data set.

symmetry and K. The K representing each peak is that at the maximum peak intensity. A similar exercise was performed using the peak intensity instead of the integrated peak area. Little difference was found in the final analysis.

The slopes obtained from Fig. 3 are proportional to the Debye-Waller factor scaled by the square of the scattering vector. Equation (8) equates this ratio to the MSD. These slopes are shown in Fig. 4 as a function of temperature. For comparison the equivalent experimental quantity extracted using Eq. (8) is also shown. What we are doing here is undoing the assumption of Eq. (8) from the original experimental analysis. This figure strongly resembles Fig. 1. The experimental data are just replotted without making the assumption of Eq. (8). What is made clear by this figure is that for both alloys calculated from model I, the model that realistically describes Pu, there is a clear positive curvature in the data. In contrast, the model II calculation, which suppressed the itinerant f-electrons, shows a slight negative curvature. If these alloys were Debye solids, the lines would have zero curvature. For the 9.8% alloy the R^2 for the linear fit (0.9689) is significantly worse than that for the quadratic fit (0.9945). Similarly for the 4.7% alloy (model I) the R^2 values were 0.8764 and 0.9864 for the linear and quadratic fits, respectively. For model II the R^2 values were 0.9599 for the linear fit and 0.9930 for the quadratic fit. Note that for model I the slopes do not approach zero at low temperature. This behavior is a result of the instability of the δ-Pu at low temperature, which leads to a static Debye-Waller factor. In contrast for model II where there is no instability, the Debye-Waller factor approaches zero at low temperature.

By examining the curvature, calculated from a fit to each curve, we can directly compare the deviations from Debye behavior. In Fig. 5 we see that the 4.7% alloy has a significant positive curvature in excellent agreement with the experimental data and the 9.8% alloy has a much smaller positive curvature. With increasing Ga concentration, the alloys become more like Debye solids. The same trend is seen in the experiment, but concentrations large enough to fully validate the calculated behavior were not examined. By sup-

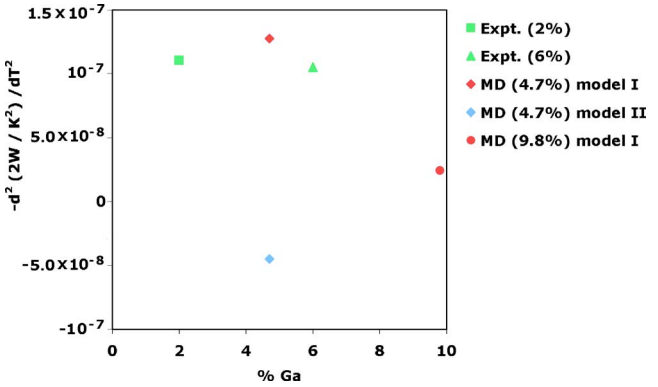

FIG. 5. (Color online) Experimental and calculated curvature of the scaled Debye-Waller factor as a function of Ga concentration.

pressing the *f*-electrons (model II) the 4.7% alloy becomes much more Debye-like. In fact, the curvature even becomes slightly negative. Both the alloying behavior and the reduction in curvature with suppression of the itinerant *f*-electrons gives good reason to believe that the unusual vibrational behavior of these alloys is controlled by the itinerant *f*-electrons. In turn, *f*-electron behavior is reflected in the lattice instability, especially at low temperature or low Ga concentration.

V. SUMMARY

Using a MEAM model of the Pu-Ga alloy system, we have calculated the MSD and neutron diffraction intensities for two Pu-Ga alloys at various temperatures. The calculated MSDs do not agree with those extracted from experimental neutron diffraction experiments, but we feel that part of the original interpretation, which was based on the Debye model, is not entirely correct. The Debye model identifies the slope of the Debye-Waller factor with respect to the square of the scattering vector as the MSD. This association is inconsistent with the calculations. The calculated MSD is linear at higher temperatures and shows an anomaly at lower temperatures due to the inherent instability of the δ phase, while the experimentally derived MSD increases quadratically.

Using a more general analysis, the deviation of the calculated and experimental neutron diffraction intensities from normal Debye behavior are found to be in reasonably good agreement. Both the experiments and the simulations substantiate the assumption that the Debye-Waller factor is proportional to the square of the scattering vector. Additions of Ga seem to drive the alloys towards normal Debye behavior. The calculations show that independent of alloy concentration or the presence of itinerant *f*-electrons, the MSD increases linearly with temperature. Thus the traditional viewpoint of a constant Debye temperature, proportional to the inverse square root of ratio of the MSD to temperature, is substantiated by the calculations.

A second MEAM model with the itinerant *f*-electrons suppressed is also used to calculate the MSD and neutron intensities. For this model both the MSD and Debye-Waller factor are found to be approximately linear with temperature. Thus the non-Debye behavior in the diffraction peaks is attributed to the presence of the itinerant *f*-electrons.

ACKNOWLEDGMENTS

The authors would like to acknowledge fruitful discussions with Sig Hecker, Blas Uberuaga, Frans Trouw, and Sven Rudin of Los Alamos National Laboratory.

[1] S. S. Hecker and L. F. Timofeeva, in *A Tale of Two Diagrams*, edited by N. G. Cooper (Los Alamos National Laboratory, Los Alamos, 2000), Vol. 1, p. 244.
[2] N. G. Cooper, in *Challenges in Plutonium Science* (Los Alamos National Laboratory, Los Alamos, 2000), http://www.fas.org/sgp/othergov/doe/lanl/pubs/number26.htm, p. 493.
[3] J. Wong, M. Krisch, D. L. Faber, F. Occelli, A. J. Schwartz, T.-C. Chiang, M. Wall, C. Boro, and R. Xu, Science **301**, 1078 (2003).
[4] X. Dai, S. Y. Sarasov, G. Kotliar, A. Migliori, H. Ledbetter, and E. Abraham, Science **300**, 953 (2003).
[5] R. J. McQueeney, A. C. Lawson, A. Migliori, T. M. Kelley, B. Fultz, M. Ramos, B. Martinez, J. C. Lashley, and S. C. Vogel, Phys. Rev. Lett. **92**, 146401 (2004).
[6] A. C. Lawson, B. Martinez, J. A. Roberts, J. J. W. Richardson, and B. I. Bennett, in *Atomic Vibrations and Melting in Plutonium*, edited by N. G. Cooper (Los Alamos National Laboratory, Los Alamos, 2000), Vol. 1, p. 190.
[7] A. C. Lawson, B. Martinez, J. A. Roberts, and B. I. Bennett, Philos. Mag. B **80**, 53 (2000).
[8] J. C. Taylor, R. G. Loasby, J. D. Dean, and P. F. Linford, in *Some Physical Properties of Plutonium at Low Temperatures*, Plutonium 1965: Proceedings of the Third International Conference on Plutonium, London, 1965, edited by A. E. Kay and M. B. Waldron (Chapman and Hall, London, 1967), p. 162.
[9] C. A. Calder, E. C. Draney, and W. W. Wilcox, J. Nucl. Mater. **97**, 126 (1981).
[10] A. Migliori, F. Freibert, J. C. Lashley, A. C. Lawson, J. P. Baiardo, and D. A. Miller, J. Supercond. **15**, 499 (2002).
[11] J. M. Wills and O. Eriksson, in *Actinide Ground State Properties—Theoretical Predictions*, edited by N. G. Cooper (Los Alamos National Laboratory, Los Alamos, 2000), Vol. 1, p. 128.
[12] M. S. Daw and M. I. Baskes, Phys. Rev. B **29**, 6443 (1984).
[13] M. S. Daw, S. M. Foiles, and M. I. Baskes, Mater. Sci. Rep. **9**, 251 (1993).
[14] M. I. Baskes, Modell. Simul. Mater. Sci. Eng. **5**, 149 (1997).
[15] J. G. Swadener, M. I. Baskes, and M. Nastasi, Phys. Rev. Lett. **89**, 085503 (2002).
[16] R. Ravelo and M. Baskes, Phys. Rev. Lett. **79**, 2482 (1997).
[17] M. I. Baskes, Phys. Rev. B **62**, 15532 (2000).
[18] M. I. Baskes, S. P. Chen, and F. J. Cherne, Phys. Rev. B **66**,

104107 (2002).
[19] M. I. Baskes, K. Muralidharan, M. Stan, S. M. Valone, and F. J. Cherne, J. Optim. Theory Appl. **55**, 41 (2003).
[20] M. I. Baskes, Phys. Rev. B **46**, 2727 (1992).
[21] M. I. Baskes, J. E. Angelo, and C. L. Bisson, Modell. Simul. Mater. Sci. Eng. **2**, 505 (1994).
[22] M. I. Baskes, Mater. Sci. Eng., A **261**, 165 (1999).
[23] S. Valone, M. Baskes, and B. Uberuaga, in *Atomistic Models of Point Defects in Plutonium Metal*, edited by G. Jarvinen (AIP, Albuquerque, 2003), Vol. 673, p. 216.
[24] B. Uberuaga, S. Valone, M. Baskes, and A. Voter, in *Accelerated Molecular Dynamics Study of Vacancies in Pu*, edited by G. Jarvinen (AIP, Albuquerque, 2003), Vol. 673, p. 213.
[25] W. G. Hoover, Phys. Rev. A **31**, 1695 (1985).
[26] S. Nose, Prog. Theor. Phys. Suppl. **103**, 1 (1991).
[27] M. Parrinello and A. Rahman, J. Appl. Phys. **52**, 7182 (1981).
[28] J. M. Ziman, *Principles of the Theory of Solids* (Cambridge University Press, Cambridge, 1964).
[29] J. E. Lynn, G. H. Kwei, W. J. Trela, V. W. Yuan, B. Cort, R. J. Martinez, and F. A. Vigil, Phys. Rev. B **58**, 11408 (1998).
[30] H. M. Ledbetter and R. L. Moment, Acta Metall. **24**, 891 (1976).
[31] J. C. Lashley, J. Singleton, A. Migliori, J. B. Betts, R. A. Fisher, J. L. Smith, and R. J. McQueeney, Phys. Rev. Lett. **91**, 205901 (2003).
[32] S. M. Valone, M. I. Baskes, M. Stan, T. E. Mitchell, A. C. Lawson, and K. E. Sickafus, J. Nucl. Mater. **324**, 41 (2004).